

Spin alignment of Quarkonia: A Possible Probe of a Deconfined QCD matter in Heavy-ion Collisions at TeV Energies

Bhagyarathi Sahoo,^{*} Captain R. Singh,[†] and Raghunath Sahoo[‡]

Department of Physics, Indian Institute of Technology Indore, Simrol, Indore 453552, India

(Dated: June 12, 2025)

In this study, we investigate the influence of deconfined QCD matter on quarkonium spin alignment in ultra-relativistic heavy-ion collisions. We estimate the spin alignment of charmonium (J/ψ , and $\psi(2S)$) and bottomonium ($\Upsilon(1S)$, and $\Upsilon(2S)$) states by calculating the energy eigenvalues in a thermal rotating medium. We solve the Schrödinger equation with a medium-modified color-singlet potential considering the coupling of spin with vorticity and magnetic field. Furthermore, we evaluate the effect of medium temperature, vorticity, magnetic field, and momentum-space anisotropy on the elements of the spin density matrix. Our findings reveal that vorticity increases the spin alignment, while the magnetic fields and anisotropy modify the observables in a state-dependent manner. These findings deepen our understanding of quarkonium spin alignment in an anisotropic magneto-vortical thermal medium, shedding light on spin transport phenomena in heavy-ion collisions.

I. INTRODUCTION

Conventionally, the thermalized deconfined state of strongly interacting partons known as quark-gluon plasma (QGP) has been investigated in heavy-ion collisions (HIC), considering the pp collisions as a baseline. It was believed that the QGP existence in pp collisions is next to impossible, as it lacks the necessary conditions for QGP to exist. However, recent studies suggest that at high multiplicity pp collisions have shown behavior similar to heavy-ion collisions, such as collective flow, strangeness enhancement, etc. [1, 2]. Moreover, few studies advocate that similar phenomena may arise in perturbative QCD-based models which do not consider the medium formation into account [3–5]. These investigations raise questions about the current QGP signatures and highlight the necessity for the next-generation probe. In the quest for such a baseline-independent probe, spin polarization comes into picture and can have implications for understanding the hot QCD matter. Studying the particle spin polarization in relativistic heavy-ion collisions may serve as a 2nd-generation probe. Recent studies present that the dilepton polarization could be a probe of thermalization of QGP [6, 7]. However, there are various sources by which particles can get polarized in ultra-relativistic nuclear collisions. Such as the vorticity field created due to the initial orbital angular momentum (OAM) in the peripheral collisions can polarize the quarks, and such polarization is transferred to the final state hadrons. The magnetic field produced by the charged spectators in such collisions interacts with the spin of the quarks and plays a vital role in heavy-quark polarization [8]. Additionally, the particle production mechanisms constrain the polarization of the hadrons

in hadronic and nuclear collisions [9]. Determining the precise contribution of each source to the spin polarization observables in ultra-relativistic collisions requires comprehensive theoretical studies with corresponding experimental observations.

The experimental measurements of global and local spin polarization of Λ and $\bar{\Lambda}$ hyperons [10–16] have been qualitatively explained using the hydrodynamic and transport models [17–22]. Apart from the spin polarization of baryons, the so-called dual observables, i.e., the spin alignment of vector mesons have been measured for K^{*0} , ϕ , D^{*+} , and K_S^0 [23–27]. Furthermore, the spin alignment of higher resonance vector mesons such as J/ψ , $\psi(2S)$, $\Upsilon(1S)$, $\Upsilon(2S)$, and $\Upsilon(3S)$ states have been measured in hadronic [28–35] and nuclear [36, 37] collisions. The measurements of spin polarization of baryons and the spin alignment of vector mesons in nuclear collisions indicate the creation of huge vorticity in the system. Thus, it is important to understand the various possible sources of vorticity formation in heavy-ion collisions.

Besides OAM, there could be several other potential sources of vorticity formation in the system. For instance, jet-like fluctuations in the expanding fireball can create smoke-loop type vortices around fast-moving particles [38]. The inhomogeneous expansion of the fireball can also generate vorticity [20, 39]. The finite viscosity present in the system can produce vorticity [40]. Furthermore, the magnetized QCD matter induces a finite rotation in the system due to the Einstein-de Haas effect [41]. The strength of the vorticity field ($\omega \approx 0.02 \text{ fm}^{-1} \approx 10^{22} \text{ s}^{-1}$) produced in heavy-ion collisions can be estimated from the average global hyperon polarization measurements of Λ and $\bar{\Lambda}$ hyperons using a statistical thermal model [42]. Recently, it has been proposed that the strength of the vorticity field can be estimated from the directed flow measurements of hadrons [43]. Accompanying the vorticity field, a

^{*} Bhagyarathi.Sahoo@cern.ch

[†] captainriturajsingh@gmail.com

[‡] Raghunath.Sahoo@cern.ch (Corresponding author)

substantial magnetic field ($eB \approx m_\pi^2 \approx 10^{18}$ G) is produced due to the charged spectators in peripheral heavy ion collisions. The strength of the magnetic field may reach up to the order of $0.1m_\pi^2$, m_π^2 , and $15m_\pi^2$ for SPS, RHIC, and LHC energies, respectively [44]. Both the vorticity field, and magnetic field provide new insights into heavy-ion collisions dynamics and significantly influence QCD thermodynamics [45, 46], transport properties [47, 48], hydrodynamic medium evolution [40], QCD phase transition [45], and spin polarization of hadrons [17–22, 49–51]. Furthermore, due to the rapid longitudinal expansion of the fireball created in heavy-ion collisions, a high degree of momentum-space anisotropy is produced in the QGP medium in its local rest frame [52]. The study of anisotropy has been a subject of investigation in various contexts [53–59]. Here, we attempted to observe the impact of medium anisotropy on the quarkonia spin alignment in heavy-ion collisions. In this article, anisotropy is introduced at the level of the medium-modified potential through Debye mass (m_D).

In ultra-relativistic heavy-ion collisions, heavy quarks are produced in the initial hard scattering, and therefore, these are considered relatively cleaner probes to investigate the early-stage properties of the hot and dense deconfined QCD medium. It can be expected that the effect of the initially produced vorticity field, magnetic field, and momentum space anisotropy strongly affects the heavy quarks compared to light quarks. Therefore, with an intense investigation of heavy-flavor hadrons at the hadronization stage, one may extract precise information about the initially produced vorticity, magnetic field, and momentum space anisotropy, and can quantify how much these affect the heavy-flavor dynamics.

In this study, we explore these effects on the spin alignment of different quarkonium states using the spin-density matrix elements, which can be measured in the experiment. The spin alignment of vector mesons has been studied by measuring the elements of a 3×3 hermitian spin density matrix ($\rho_{m,m'}$), where m and m' label the spin component along the quantization axis. The diagonal elements ρ_{11} , ρ_{00} , and ρ_{-1-1} define the probabilities of the spin component of vector mesons along the quantization axis. Out of these three diagonal elements, ρ_{00} is independent and can be measured in experiments in two-body decays to pseudoscalar mesons. In the absence of spin alignment, all three spin states of vector mesons 1, 0, and -1 are equally probable, and thus $\rho_{00} = 1/3$. The deviation of ρ_{00} from $1/3$ (i.e. $\rho_{00} - 1/3$) determines the degree of alignment of vector meson. On the other hand, the off-diagonal elements of the spin density matrix play a critical role in understanding the spin alignment of quarkonium states in the QGP medium. The diagonal component ρ_{00} is commonly used to quantify spin alignment, indicating the probability of finding a vector meson in a spin-0

projection along a chosen quantization axis, while the off-diagonal elements such as $\rho_{1,-1}$, $\rho_{-1,0}$, and $\rho_{1,0}$ provide information about the quantum coherence and interference between different spin states. The non-zero off-diagonal elements imply that the system is in a superposition of spin states rather than a statistical mixture, thus emphasizing the partial coherence and entanglement within the spin degrees of freedom. These coherence terms are sensitive to the microscopic structure and dynamics of the medium. For instance, in a locally rotating QGP, vorticity gradients may induce spin-orbit couplings that lead to position-dependent polarization, referred to as local spin alignment. This effect cannot be captured solely by ρ_{00} , which represents global polarization. Instead, the angular modulations introduced by off-diagonal terms such as $\rho_{1,-1}$ and $\rho_{1,0}$ become crucial in distinguishing local from global alignment. Specifically, $\rho_{1,-1}$ contributes to azimuthal anisotropies in the decay distributions of vector mesons, while $\rho_{-1,0}$ and $\rho_{1,0}$ encode spin correlations along transverse directions. They may also provide valuable insights into medium-induced spin correlations, the local spin structure, and non-equilibrium QCD dynamics. The measurement of these elements is embedded in experimental analyses, when a vector meson decays, such as $J/\psi \rightarrow \mu^+\mu^-$, angular distribution in the rest frame of the decaying particle defined using the coefficients λ_θ , λ_ϕ , and $\lambda_{\theta\phi}$ which are directly related to ρ_{00} , $\rho_{1,-1}$, and a linear combination of $\rho_{1,0}$ and $\rho_{-1,0}$, respectively. Through experimental fits to such distributions, one can extract these elements and obtain a more complete description of the spin polarization.

Various phenomenological approaches have been developed gradually to describe the spin alignment phenomena of vector mesons [60–78]. The global quark polarization leads to the spin alignment of vector mesons was first introduced in Ref. [60]. A quark coalescence model attempts to explain the spin alignment of vector mesons in Refs. [61, 62]. Apart from the global spin alignment, the local spin alignment induced by the local vorticity is discussed in Ref. [63]. The authors have proposed that the measurement of ρ_{00} observable as a function of the azimuthal angle of the particle's transverse momentum with respect to the reaction plane, off-diagonal elements of the spin-density matrix $\rho_{m,m'}$, and $\langle \rho_{00} \rangle$ with respect to different event planes can be used to separate the local spin alignment of vector mesons from the global one. In Ref. [66–68], the authors have argued that the spin alignment of vector mesons can serve as a probe of spin-hydrodynamics and freeze-out with a coalescence model. The spin alignment of vector mesons is explained with the anisotropies of local field correlation (or fluctuation of vector meson force field) [69, 70], glasma field [71, 72], light front quarks [73], local spin density fluctuations [74], holographic method [75, 76], hadronization mechanisms [77, 78], etc.

In this study, we explore the spin alignment of various charmonium states; such as J/ψ , and $\psi(2S)$, as well as bottomonium states; such as $\Upsilon(1S)$, and $\Upsilon(2S)$ as a function of transverse momentum (p_T). We investigate the effect of medium rotation or vorticity (ω), magnetic fields (eB), and momentum space anisotropy (ξ) on the spin alignment observables. We estimate both the diagonal and off-diagonal elements of the spin-density matrix for quarkonia in a thermal rotating medium. To obtain these matrix elements, we solved the Schrödinger equation numerically and obtained the energy eigenvalues using a medium-modified color octet potential model for quarkonia. We extend the standard formalism of solving quarkonium states in a rotating frame to account for the external magnetic field and medium anisotropy. The energy eigenvalues depend upon the coupling of spin with rotation and magnetic field.

This paper is organized as follows: Section II provides a detailed description of the formalism used in this study, Section III discusses the results, and Section IV offers a summary of our findings.

II. FORMULATION

In the present study, we assume the quarkonium states as quantum particles, and it is characterized by the quantum wavefunction. The real-time evolution of quarkonium states is described using the time-dependent Schrödinger equation (SE) with a temperature-dependent complex heavy-quark potential. This formalism has been widely used to describe the evolution, production, and suppression of various quarkonium states in heavy-ion and small collision systems at various center of mass energies [79–84]. In this work, we use the standard developed formalism and investigate the spin-alignment of quarkonium states by incorporating the spin-vorticity and spin-magnetic field coupling in a thermal rotating medium.

Now, before we explore the quarkonium spin alignment mechanism within the QGP medium, it is necessary to first examine how the quarkonium Hamiltonian is modified in the medium in the presence of vorticity, temperature, and magnetic field. It is well established that the Hamiltonian of a charged particle with charge q , mass m , and spin S , moving in a rotating medium with angular velocity ω and subjected to a magnetic field B , can be expressed as [85–87];

$$\mathcal{H} = \frac{1}{2m} (\mathbf{p} - q\mathbf{A} - m\boldsymbol{\omega} \times \mathbf{r})^2 - \frac{m}{2} (\boldsymbol{\omega} \times \mathbf{r})^2 - \boldsymbol{\mu} \cdot \mathbf{B} - \boldsymbol{\omega} \cdot \mathbf{S} + V(r) \quad (1)$$

Here, $\boldsymbol{\omega} \cdot \mathbf{S}$ term arises from the coupling between the rotation of the system and the spin of the particle, while the term $\boldsymbol{\mu} \cdot \mathbf{B}$ results from the coupling between the

magnetic field and the spin magnetic dipole moment. The $\mathbf{A} = -\frac{1}{2}(\mathbf{r} \times \mathbf{B})$, denotes the magnetic vector potential, and $\boldsymbol{\mu}$ stands for the magnetic moment associated with the spin of a particle with charge q and mass m . The magnetic moment is defined as $\boldsymbol{\mu} = g\frac{q}{2m}\mathbf{S}$, where g is the Land'e g -factor.

Now, for a two-body system like quarkonia in QGP medium, Eq. 1 can be written as;

$$\mathcal{H} = \sum_{i=1,2} \left[\frac{1}{2m_i} (\mathbf{p}_i - q_i\mathbf{A}_i - m_i\boldsymbol{\omega}_i \times \mathbf{r}_i)^2 - \frac{m_i}{2} (\boldsymbol{\omega}_i \times \mathbf{r}_i)^2 - \boldsymbol{\mu}_i \cdot \mathbf{B}_i - \boldsymbol{\omega}_i \cdot \mathbf{S}_i \right] + V(|\mathbf{r}_1 - \mathbf{r}_2|) \quad (2)$$

In this study, the index i runs over 1 and 2, representing the heavy quark and antiquark, respectively. Employing the standard reduction procedure of a two-body system to an effective one-body description in the center of the mass frame and introducing the corresponding reduced coordinate system, the dynamics of the quarkonia can be expressed through the following relation,

$$\begin{cases} \mathbf{P} = \mathbf{p}_1 + \mathbf{p}_2, & \mathbf{p} = m_\mu \left(\frac{\mathbf{p}_1}{m_1} - \frac{\mathbf{p}_2}{m_2} \right) \\ m_\mu = \frac{m_1 m_2}{m_1 + m_2}, \\ \mathbf{r}_1 = \mathbf{R} + \frac{m_2}{m_1 + m_2} \mathbf{r}, & \mathbf{r}_2 = \mathbf{R} - \frac{m_1}{m_1 + m_2} \mathbf{r} \end{cases} \quad (3)$$

where, $m_\mu = m_Q/2$ represents the reduced mass in the center of mass frame of the heavy-quark pair, with the charm quark mass $m_c = 1.27$ GeV and bottom quark mass $m_b = 4.18$ GeV. We assume that the quark and anti-quark pair forming the quarkonium states exist within the same vortical and magnetic fields. Thus, we have $\boldsymbol{\omega}_1 = \boldsymbol{\omega}_2 = \boldsymbol{\omega}$ and $\mathbf{B}_1 = \mathbf{B}_2 = \mathbf{B}$, and following this, the Hamiltonian can be rewritten as,

$$\mathcal{H} = \frac{P^2}{2M} + \frac{p^2}{2m_\mu} - \mathbf{P} \cdot (\boldsymbol{\omega} \times \mathbf{R}) - \mathbf{p} \cdot (\boldsymbol{\omega} \times \mathbf{r}) - (\boldsymbol{\mu}_1 + \boldsymbol{\mu}_2) \cdot \mathbf{B} - \boldsymbol{\omega} \cdot (\mathbf{S}_1 + \mathbf{S}_2) + V(|\mathbf{r}|) \quad (4)$$

Since we are interested in the reduced coordinate, we obtain

$$\mathcal{H} = \frac{p^2}{2m_\mu} - \mathbf{p} \cdot (\boldsymbol{\omega} \times \mathbf{r}) - (\boldsymbol{\mu}_1 + \boldsymbol{\mu}_2) \cdot \mathbf{B} - \boldsymbol{\omega} \cdot (\mathbf{S}_1 + \mathbf{S}_2) + V(|\mathbf{r}|) \quad (5)$$

Assuming the magnetic field \mathbf{B} and the rotation $\boldsymbol{\omega}$ along the z direction, such that $\mathbf{B} = B\hat{z}$ and $\boldsymbol{\omega} = \omega\hat{z}$, the Eq. 5, can be written as;

$$\mathcal{H} = \frac{p^2}{2m_\mu} - \mathbf{p} \cdot (\boldsymbol{\omega} \times \mathbf{r}) - \frac{qB}{2m} (S_{1z} - S_{2z}) - \omega (S_{1z} + S_{2z}) + V(|\mathbf{r}|) \quad (6)$$

Writing $\mathbf{p} = -i\nabla$, $\mathcal{H} = i\frac{\partial}{\partial t}$, $L_z = -i\frac{\partial}{\partial\phi}$, $S_{1z} + S_{2z} = S_z$, we can rewrite the Eq. 6 as

$$i\frac{\partial}{\partial t} = -\frac{1}{2m_\mu}\nabla^2 - \omega(L_z + S_z) - \frac{qB}{2m}(S_{1z} - S_{2z}) + V(|\mathbf{r}|) \quad (7)$$

Expressing the Laplacian operator in spherical coordinates and following the separation of the variable method, the radial part of the Schrödinger equation can be written as;

$$\frac{1}{r^2}\frac{d}{dr}\left(r^2\frac{dR(r)}{dr}\right) + 2m_\mu\left[(E - V(r)) - \frac{l(l+1)}{2m_\mu r^2} - \omega(L_z + S_z) - \frac{qB}{m_\mu}(S_{1z} - S_{2z})\right]R(r) = 0 \quad (8)$$

To solve the Schrödinger equation in the presence of rotation, we define ω in terms of the conserved circulation C ,

$$C = \oint \vec{v} \cdot d\vec{l} \quad (9)$$

Applying the fundamental theorem for curl, which goes by the special name of Stokes' theorem, states that the line integral can be converted into a surface integral. Thus, Eq. 9 can be written as;

$$C = \oint \vec{\nabla} \times \vec{v} \cdot d\vec{S} = 2\omega\pi r^2 \quad (10)$$

where, $\vec{\omega} = \frac{1}{2}\vec{\nabla} \times \vec{v}$ is the non-relativistic vorticity. Here, we assume the rotation to be classical and can be related to the hydrodynamic vorticity, such as the thermal vorticity, temperature vorticity, and enthalpy vorticity, etc.

Substituting the value of C in Eq. 8, we obtain

$$\frac{1}{r^2}\frac{d}{dr}\left(r^2\frac{dR(r)}{dr}\right) + 2m_\mu\left[(E - V(r)) - \frac{l(l+1)}{2m_\mu r^2} - \frac{m_j C}{2\pi r^2} - \frac{qB}{m_\mu}\right]R(r) = 0 \quad (11)$$

The color singlet potential for $c - \bar{c}$ bound state in the QGP as follows [88];

$$V(r, m_D) = \frac{\sigma}{m_D}(1 - e^{-m_D r}) - \alpha_{\text{eff}}\left(m_D + \frac{e^{-m_D r}}{r}\right) - i\alpha_{\text{eff}}T \int_0^\infty \frac{2z dz}{(1+z^2)^2} \left(1 - \frac{\sin(m_D r z)}{m_D r z}\right) \quad (12)$$

Where the first and second terms on the right-hand side are the string term and the coulombic term, respectively. The third term on the right-hand side is the imaginary part of the heavy-quark potential. In the above Eq. 12 :

- σ is the string tension constant between $c\bar{c}$ bound state, and is given as $\sigma = 0.192 \text{ GeV}^2$.
- T_{eff} is the effective temperature of quarkonia in the medium arises due to the Relativistic Doppler Shift (RDS), and it is given as [79];

$$T_{\text{eff}}(p_T) = \frac{T\sqrt{1-|v_r|^2}}{2|v_r|} \ln\left[\frac{1+|v_r|}{1-|v_r|}\right] \quad (13)$$

Here, v_r is the relative velocity between the medium and quarkonia. For a more detailed discussion on effective temperature, see the Refs. [79–81, 89, 90]

- m_D is the Debye mass. In the deconfined medium, Debye mass has contributions from both the gluon and quark degrees of freedom, and is expressed as;

$$m_D(T) = T\sqrt{4\pi\alpha_s(\Lambda^2)\left(\frac{N_c}{3} + \frac{N_f}{6}\right)} \quad (14)$$

here, $\alpha_s(\Lambda^2)$ is the temperature-dependent strong running coupling constant,

$$\alpha_s(\Lambda^2) = \frac{1}{b_1 \ln\left(\frac{\Lambda^2}{\Lambda_{\overline{MS}}^2}\right)} \quad (15)$$

where $b_1 = \frac{11N_c - 2N_f}{12\pi}$, $\Lambda_{\overline{MS}} = 0.176 \text{ GeV}$ for $N_f = 3$ and renormalization scale $\Lambda = 2\pi T$.

- α_{eff} is effective coupling constant, depending on the strong coupling constant at soft scale $\alpha_s^s = \alpha_s(m_c\alpha_s/2)$, given as $\alpha_{\text{eff}} = \frac{4}{3}\alpha_s^s$.

We solve Eq. 11 numerically by taking a 10^4 point logarithmically spaced finite spatial grid. The quarkonium wave functions and corresponding energy eigenvalues are obtained using temperature-dependent potential as defined in Eq. 12. The relativistic corrections to the potential model are neglected during the evolution of quarkonium states due to the large mass of charm and bottom quarks. As Eq. 12 indicates, the energy eigenvalues and quarkonium wave function depend on the Debye mass. Hence, in principle, any change in the Debye mass will change the eigenvalues and wave function. In this study, we consider two physical scenarios; first, we discuss the Debye mass in the presence of an external magnetic field, and then the Debye mass in the presence of momentum-space anisotropy.

A. Debye Mass under Strong Magnetic Field

In the presence of a magnetic field, the change brought to the Debye mass arises from the quark loop, as gluons do not interact with the magnetic field. The total Debye

mass of partons in a strong magnetic field has been calculated using the temporal component of the vacuum self-energy diagram at the static limit. It is given as [91, 92].

$$m_D^2(T, eB) = 4\pi\alpha_s(\Lambda^2, |eB|) \left[T^2 \frac{N_c}{3} + \sum_f \frac{|q_f eB|}{4\pi^2} \right] \quad (16)$$

here, $\alpha_s(\Lambda^2, |eB|)$ is the modified running coupling constant, depending on the magnetic field and temperature. It can be written as [93, 94],

$$\alpha_s(\Lambda^2, |eB|) = \frac{g_s^2}{4\pi} = \frac{\alpha_s(\Lambda^2)}{1 + b_1 \alpha_s(\Lambda^2) \ln \left(\frac{\Lambda^2}{\Lambda^2 + |eB|} \right)} \quad (17)$$

B. Effect of Anisotropy on Debye Mass

Inhomogeneity in momentum space distribution between longitudinal and transverse directions gives rise to the momentum space anisotropy in relativistic heavy-ion collisions. This anisotropy certainly affects the Debye mass, therefore, in the presence of momentum space anisotropy Debye mass is factorized as [52, 95–99];

$$m_D(T, \xi) = m_D(T) \left[f_1(\xi) \cos^2 \theta + f_2(\xi) \right]^{-\frac{1}{4}} \quad (18)$$

Here, parameter ξ measures the degree of momentum-space anisotropy, defined as;

$$\xi = \frac{1}{2} \frac{\langle \mathbf{k}_\perp^2 \rangle}{\langle k_z^2 \rangle} - 1 \quad (19)$$

where $k_z \equiv \mathbf{k} \cdot \mathbf{n}$, $\mathbf{k}_\perp \equiv \mathbf{k} - \mathbf{n}(\mathbf{k} \cdot \mathbf{n})$ correspond to the particle momenta along and perpendicular to the direction of anisotropy, and θ is the angle between particle momentum (\mathbf{k}) with respect to direction of anisotropy (\mathbf{n}). Here, we assume a classical picture in which the direction of anisotropy is along the direction of the particle. The $f_1(\xi)$ and $f_2(\xi)$ are parameterized in such a way that Eq. 18 remains always true under small and large values of ξ . Here, it is worth mentioning that the parametrization of the anisotropic Debye mass for arbitrary ξ is obtained by constructing a model for the real part of short-range heavy quark-antiquark potential [96].

$$f_1(\xi) = \frac{9\xi(1+\xi)^{\frac{3}{2}}}{2\sqrt{3} + \xi(3+\xi^2)} \times \frac{\pi^2(\sqrt{2} - (1+\xi)^{\frac{1}{8}}) + 16(\sqrt{3+\xi} - \sqrt{2})}{(\sqrt{6} - \sqrt{3})\pi^2 - 16(\sqrt{6} - 3)} \quad (20)$$

$$f_2(\xi) = \xi \left(\frac{16}{\pi^2} - \frac{\sqrt{2}(\frac{16}{\pi^2} - 1) + (1+\xi)^{\frac{1}{8}}}{\sqrt{3+\xi}} \right) \left(1 - \frac{(1+\xi)^{\frac{3}{2}}}{1 + \frac{\xi^2}{3}} \right) + f_1(\xi) + 1 \quad (21)$$

So far, we have set up the effective Hamiltonian for quarkonium states in a rotating, magnetized, and anisotropic QCD medium, incorporating spin-vorticity and spin-magnetic couplings along with the potential. It has also been discussed how the Debye mass modifies in the presence of the magnetic field and momentum-space anisotropy. With this configuration in place, we now discuss the spin-alignment of quarkonia in the QGP medium.

C. Quarkonia Spin Alignment

The spin density operator can be written as

$$\hat{\rho} = e^{-\beta \hat{H}}, \quad \beta = \frac{1}{T} \quad (22)$$

here, \hat{H} is the Hamiltonian operator. The spin density matrix in a rotating frame with angles θ_r and ϕ_r can be transformed as;

$$\hat{\rho}^r(\theta_r, \phi_r) = U(\theta_r, \phi_r) \hat{\rho} U(\theta_r, \phi_r)^{-1} \quad (23)$$

where

$$U(\theta_r, \phi_r) = D(\alpha, \beta, \gamma) = \exp\left(\frac{-iJ_x \alpha}{\hbar}\right) \exp\left(\frac{-iJ_y \beta}{\hbar}\right) \times \exp\left(\frac{-iJ_z \gamma}{\hbar}\right) \quad (24)$$

Taking $\alpha = \phi_r$, $\beta = \theta_r$, and $\gamma = 0$, Eq. 24 can be written as,

$$D_{m,m'}^j(\phi_r, \theta_r) = \langle j, m | D(\phi_r, \theta_r, 0) | j, m' \rangle \quad (25)$$

with

$$D_{m,m'}^j(\phi_r, \theta_r) = e^{-im\phi_r} d_{m,m'}^j(\theta_r) \quad (26)$$

$$\left[D_{m,m'}^j(\phi_r, \theta_r) \right]^{-1} = e^{im\phi_r} \left[d_{m,m'}^j(\theta_r) \right]^{-1} \quad (27)$$

For $j = 1$, we have explicitly

$$d^1(\theta_r) = \begin{pmatrix} \frac{1}{2}(1 + \cos \theta_r) & -\frac{1}{\sqrt{2}} \sin \theta_r & \frac{1}{2}(1 - \cos \theta_r) \\ \frac{1}{\sqrt{2}} \sin \theta_r & \cos \theta_r & -\frac{1}{\sqrt{2}} \sin \theta_r \\ \frac{1}{2}(1 - \cos \theta_r) & \frac{1}{\sqrt{2}} \sin \theta_r & \frac{1}{2}(1 + \cos \theta_r) \end{pmatrix} \quad (28)$$

We can expand the right-hand side of Eq. 23,

$$\hat{\rho}_{m,m'}^r(\theta_r, \phi_r) = \sum_{m'', m'''} \langle j, m | D | j, m'' \rangle \langle j, m'' | \hat{\rho} | j, m''' \rangle \times \langle j, m''' | D^{-1} | j, m' \rangle \quad (29)$$

$$\begin{aligned}
&= \sum_{m'', m'''} e^{-im\phi_r} d_{m, m''}^j(\theta_r) \langle j, m'' | \hat{\rho} | j, m''' \rangle \\
&\quad \times e^{im'''\phi_r} \left[d_{m''', m'}^j(\theta_r) \right]^{-1} \\
&= \sum_{m'', m'''} e^{i(m'''-m)\phi_r} d_{m, m''}^j(\theta_r) \rho_{m'', m'''} \left[d_{m''', m'}^j(\theta_r) \right]^{-1}
\end{aligned} \tag{30}$$

and

$$\rho_{m'', m'''} = \langle j, m'' | \hat{\rho} | j, m''' \rangle = \frac{1}{Z} e^{-\beta E_{m'''}} \delta_{m'', m'''} \tag{31}$$

Where Z is the normalization factor corresponding to the spin density matrix and $Z = \text{Tr}(\rho)$.

Employing the above-developed formalism, we now estimate the diagonal and off-diagonal elements of the spin-density matrix for quarkonium states in a rotating, magnetized, and anisotropic medium. The value of θ_r and ϕ_r used in Eq. 30 are taken from Ref. [67], where these parameters are determined by solving a system of equations in Collins-Soper frame to J/ψ and Υ states with respective ranges $4.0 < p_T < 6.0$ GeV/c and $p_T > 15$ GeV/c. The value of $\theta_r = 1.75 \pm 0.10$ rad for J/ψ and $\theta_r = 1.58 \pm 0.10$ rad for Υ states. The off-diagonal elements are obtained using $\phi_r = 0$.

III. RESULTS AND DISCUSSION

As discussed in the previous section, the energy eigenvalues used to calculate the spin alignment factor depend on the medium temperature, rotation, magnetic field, and anisotropy parameter. The different values of medium temperature, rotation, magnetic field, and anisotropy parameters are considered for this study. In this section, first, we will investigate the effect of medium rotation quantified in terms of the circulation parameter C on the diagonal elements of the spin density matrix, i.e., ρ_{00} for different quarkonium states. Then we will investigate the effect of medium temperature (T), external magnetic field (eB), and momentum-space anisotropy (ξ) on ρ_{00} observable. Furthermore, we will explore a few off-diagonal elements of the spin-density matrix for quarkonium states to have a complete understanding of spin-vorticity coupling dynamics in relativistic heavy-ion collisions.

A. Diagonal elements

Using Eq. 30, one can obtain the 00^{th} diagonal elements of the spin-density matrix in a rotating frame, ρ_{00}^r , and is expressed as follows;

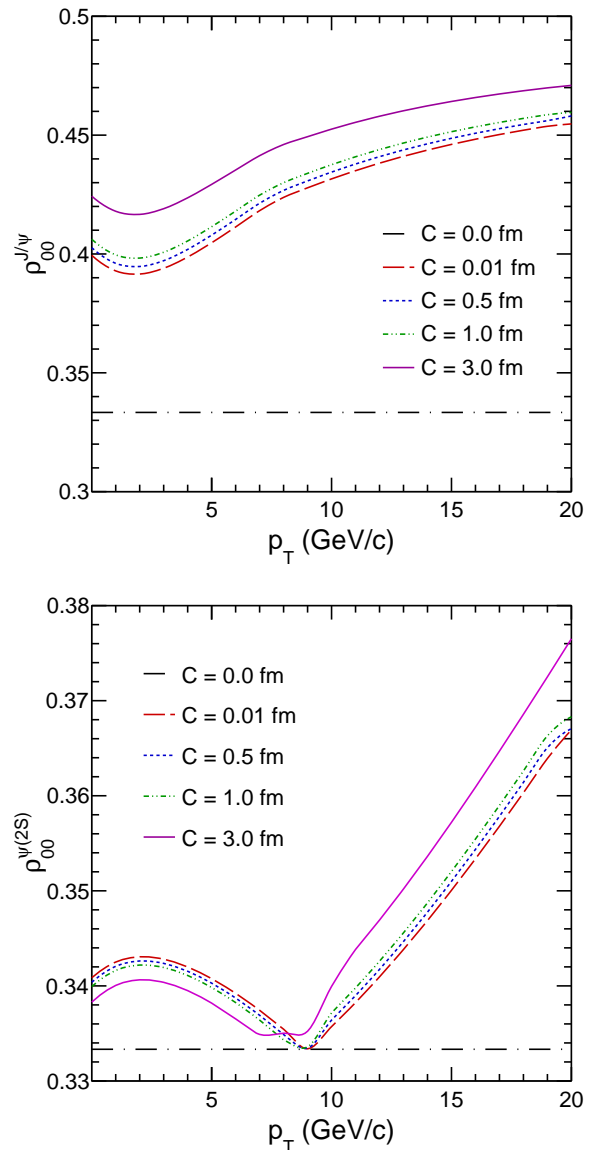


FIG. 1. (Color online) The spin alignment observable ρ_{00} as a function of p_T for J/ψ (upper panel) and $\psi(2S)$ (lower panel) for different values of the circulation parameter, C using $T = 0.175$ GeV.

$$\rho_{00}^r = \frac{1}{Z} \left[\cos^2 \theta_r e^{-\beta E_0} + \frac{1}{2} \sin^2 \theta_r (e^{-\beta E_1} + e^{-\beta E_{-1}}) \right] \tag{32}$$

Figure 1 shows 00^{th} -elements of the spin-density matrix, ρ_{00} ¹, as a function of transverse momentum p_T for various values of C at $T = 0.175$ GeV. The black

¹ It is important to note that throughout the study we use ρ_{00}^r as ρ_{00} , for simplicity. So, by ρ_{00} we mean the 00^{th} -elements of the spin-density matrix ρ in rotating frame.

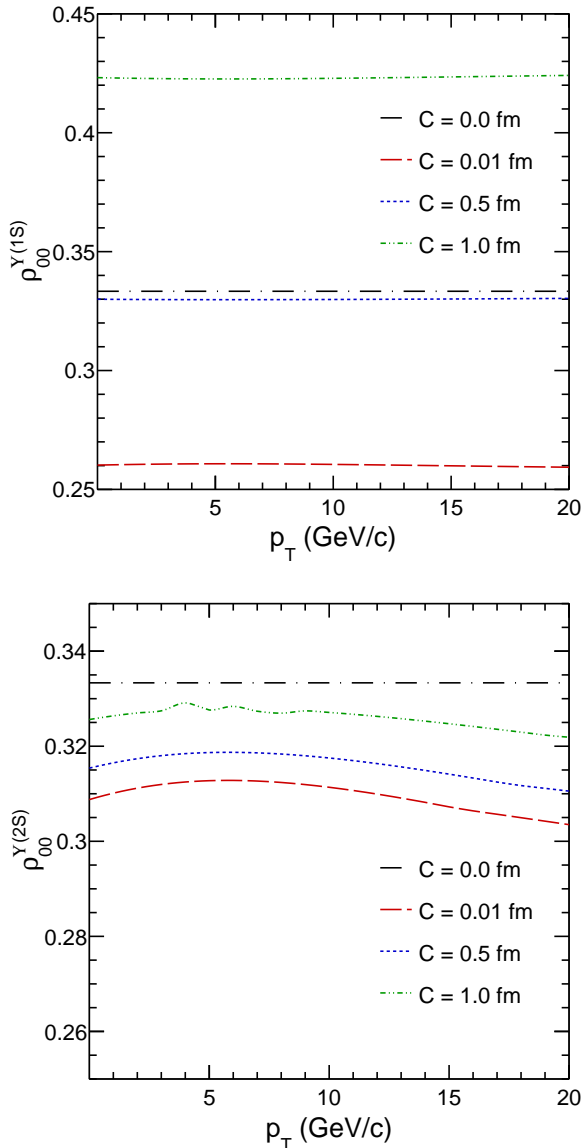


FIG. 2. (Color online) The spin alignment observable ρ_{00} as a function of p_T for $\Upsilon(1S)$ (upper), and $\Upsilon(2S)$ (lower) for different values of the circulation parameter, C using $T = 0.175$ GeV.

dashed line in Fig. 1 and other figures as well represent a thermal irrotational medium ($C = 0$), for which ρ_{00} is $1/3$. This black dashed line serves as the baseline value for the spin alignment study. Any deviation from the baseline value $\rho_{00} = 1/3$ depicts the degree of alignment of the particle spin in a preferential direction. The upper and lower panels of Fig. 1 demonstrate the J/ψ and $\psi(2S)$ spin alignment with p_T , respectively. Here, p_T -dependence in spin alignment observable ρ_{00} is incorporated through T_{eff} , which is used to estimate the quarkonium temperature in the medium. The T_{eff} is a result of relativistic Doppler shift, initially T_{eff} increases up to $p_T \sim 3$ GeV/c and afterward decreases with

increasing p_T . It has been used to obtain the energy eigenvalue, which is subsequently employed to determine quarkonium spin alignment. As a consequence, the spin alignment observable ρ_{00} for J/ψ initially decreases up to $p_T \sim 3$ GeV/c as shown in the upper panel of Fig. 1. At $p_T \gtrsim 4$ GeV/c, spin alignment increases with increasing p_T . Further, for the given p_T values, ρ_{00} increases with increasing circulation parameter C . The information about vorticity is encoded in the conserved circulation parameter, C . The coupling between quarkonium spin and medium vorticity enhances the quarkonium stability in the medium by lowering its eigenenergy. The effect of medium vorticity was found to be marginal for $\omega \leq 0.16$ fm $^{-1}$ (corresponds to $C = 1$ fm, and $r = 1$ fm). However, with increasing vorticity or C , $\rho_{00}^{J/\psi}$ increases without changing the pattern as a function of p_T .

The spin alignment of $\psi(2S)$ is shown in the lower panel of Fig. 1, demonstrates a slight increase in ρ_{00} at $p_T \leq 2$ GeV/c. At these low p_T values, the $\psi(2S)$ is supposedly moving slower than the surrounding medium, resulting in a reduced T_{eff} which in turn reduces the eigenenergy, leading to an increase in ρ_{00} . Consequently, we observe an increasing trend in ρ_{00} with the initial p_T values. For the intermediate p_T range, i.e. $2 < p_T < 9$ GeV/c, $\psi(2S)$ moves more coherently with medium. This results in an increase in T_{eff} and so the eigenenergy, causing ρ_{00} to decrease within this p_T range. The $\psi(2S)$ being an excited state has a relatively high eigenenergy that makes it relatively unstable and less susceptible to polarize in the medium. Hence, its spin alignment remains small compared to J/ψ . In terms of the circulation parameter, C , $\psi(2S)$ shows a different spin alignment pattern than J/ψ , at $p_T \lesssim 9$ GeV/c, i.e., the ρ_{00} matrix element decreases with C . This can be attributed to a complex interplay between medium vorticity and T_{eff} . However, for $p_T > 9$ GeV/c, the spin alignment behavior of $\psi(2S)$ tends to follow a trend similar to J/ψ , although the relative difference of ρ_{00} from the baseline value is small for $\psi(2S)$.

Similarly, in Fig. 2 we have shown the spin alignment of $\Upsilon(1S)$ (upper panel), and $\Upsilon(2S)$ (lower panel) for various values of C at $T = 0.175$ GeV. As $\Upsilon(1S)$ is a massive and tightly bound state, it has small eigen energies, which give rise to the large spin polarization for very small and large values of C , i.e., $C = 0.01$ fm and 1.0 fm. Around $C = 0.5$ fm, it predicts negligible polarization for $\Upsilon(1S)$, as $\rho_{00} \approx \frac{1}{3}$. The infinitesimal dependence of ρ_{00} on p_T exhibits that $\Upsilon(1S)$ is a highly stable particle and any changes brought in its eigenenergy by T_{eff} at $T = 0.175$ GeV, remains almost ineffective. On the other hand, ρ_{00} for $\Upsilon(2S)$ shown in the lower panel of Fig. 2 varies with p_T . The spin alignment pattern of $\Upsilon(2S)$ follows the same explanation as given for $\psi(2S)$ at $p_T < 9$ GeV/c. However, for $\Upsilon(2S)$ state p_T range is extended to $p_T \geq 20$ GeV/c because of its larger mass compared with $\psi(2S)$. The degree of spin alignment is found to decrease with

the considered circulation parameter C .

It is noteworthy to mention, that ρ_{00} is more sensitive to C for $\Upsilon(1S)$ state compared to $\Upsilon(2S)$ states. For example, for $\Upsilon(1S)$ state at $C = 0.01$ fm, the deviation of ρ_{00} from the baseline value $1/3$ ($\rho_{00} < 1/3$) is smaller, while at $C = 1.0$ fm, it is greater than $1/3$ ($\rho_{00} > 1/3$). It indicates that the shape of the angular distribution of the Υ state flips with the anisotropy created due to the medium vorticity. Since ρ_{00} is closely related to the polarization parameter λ_θ , this change reflects a transition from transverse to longitudinal spin polarization. The value of vorticity at which this transition occurs is highly sensitive to the temperature and equilibration time of the quark-gluon plasma. Hence, the spin alignment (or angular distribution) of the $\Upsilon(1S)$ state may serve as a probe of system thermalization and could potentially be used to estimate the equilibration time. The deviation of ρ_{00} from the $1/3$ baseline value is negative for the $\Upsilon(2S)$ state for all considered values of C . However, there is a clear trend that with increasing C , the ρ_{00} value approaches $1/3$. At higher C , it is expected $\Upsilon(2S)$ has similar features as $\Upsilon(1S)$.

A comparison for the order of spin alignment for J/ψ ,

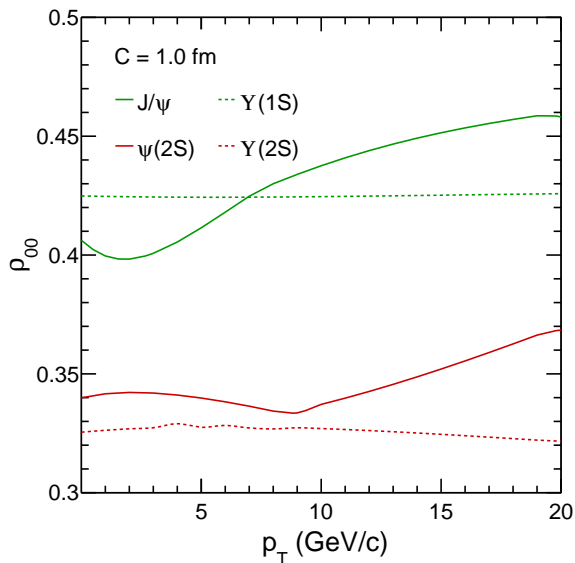


FIG. 3. (Color online) The spin alignment observable ρ_{00} as a function of p_T for J/ψ , $\psi(2S)$, $\Upsilon(1S)$, and $\Upsilon(2S)$ states at the circulation parameter, $C = 1.0$ fm using $T = 0.175$ GeV.

$\psi(2S)$, $\Upsilon(1S)$, and $\Upsilon(2S)$ as the function of p_T is shown in Fig. 3 at $C = 1.0$ fm. Charmonium states exhibit an increasing trend in ρ_{00} with p_T , indicating that unperturbed particles are most likely to polarize in the medium. While ρ_{00} for bottomonium states remains constant over whole p_T . At $p_T \lesssim 7$ GeV/c, the order of spin alignment of J/ψ is smaller than $\Upsilon(1S)$, because perturbation in the state is large at low p_T , which decrease with increasing p_T . As a result, for $p_T > 7$ GeV/c, the order of spin alignment of J/ψ becomes larger than

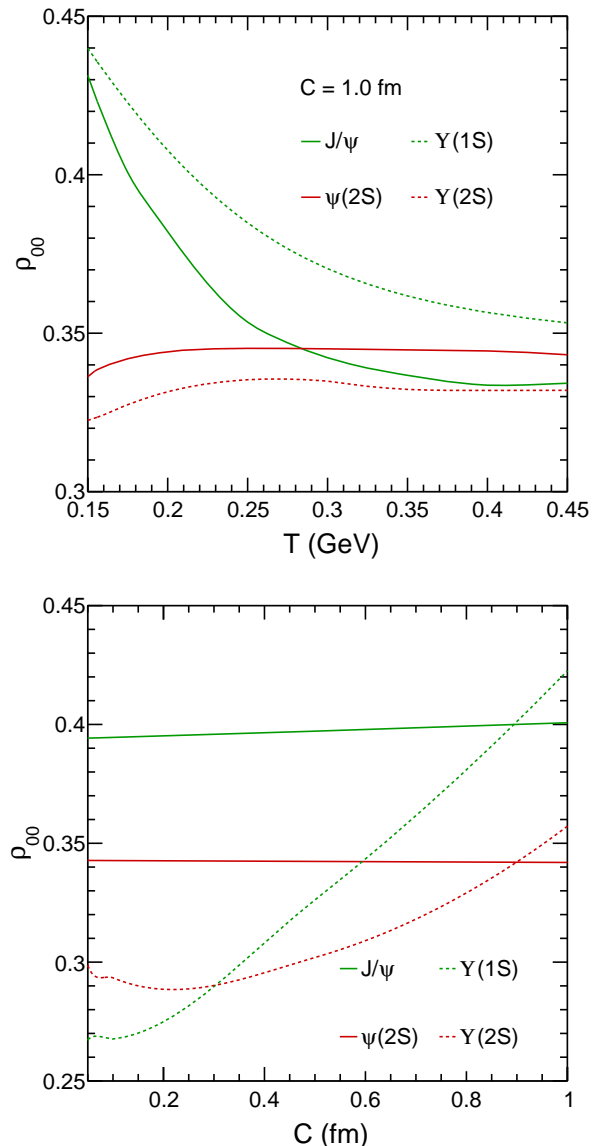


FIG. 4. (Color online) The spin alignment of quarkonium states such as J/ψ , $\psi(2S)$, $\Upsilon(1S)$, and $\Upsilon(2S)$ states are shown in the upper and lower panels of the figure. The upper panel represents the spin alignment observable ρ_{00} as a function of temperature T at a conserved circulation $C = 1.0$ fm. The lower panel depicts the spin alignment as a function of C obtained at $T = 0.175$ GeV.

$\Upsilon(1S)$. It can also be inferred that relatively lighter mass particles with almost the same binding energy are more prone to polarize in the medium. Among all, J/ψ shows the largest deviation from the unpolarized baseline ($\rho_{00} = 1/3$) at high p_T , followed by $\psi(1S)$ state. While $\psi(2S)$ shows a moderate spin alignment and $\Upsilon(2S)$ remains the least polarized, with ρ_{00} values closer to $1/3$.

Figure 4 depicts the spin alignment when particles are at rest in the medium and explicitly explores the

temperature and vorticity dependence. The upper panel of Fig. 4 displays the variation of ρ_{00} as a function of temperature T for J/ψ , $\psi(2S)$, $\Upsilon(1S)$, and $\Upsilon(2S)$ states at $C = 1.0$ fm. The results indicate that the spin alignment of the quarkonium 1S states exhibits a notable sensitivity to the medium temperature. In particular, ρ_{00} decreases with increasing temperature for both J/ψ and $\Upsilon(1S)$. This behavior can be attributed to the rapid increase in the magnitude of the eigen energies of these states at high temperatures, which renders them progressively unstable. However, $\Upsilon(1S)$, having a higher binding energy compared to J/ψ , retains a finite spin alignment even at high temperatures, with $\rho_{00} > \frac{1}{3}$. In contrast, the spin alignment for J/ψ diminishes with temperature, approaching the unpolarized limit of $\rho_{00} \sim \frac{1}{3}$. We found the deviation of ρ_{00} from $1/3$ is a small positive value for $\psi(2S)$ and has a mild dependence as a function of temperatures. This is because the energy eigenvalues have a marginal dependence as a function of temperature. Similarly, for the $\Upsilon(2S)$ states, ρ_{00} exhibits only a marginal dependence on temperature up to $T \approx 270$ MeV, beyond which it tends to saturate towards $1/3$.

The lower panel of Fig. 4 illustrates the dependence of ρ_{00} on the parameter C for the aforementioned quarkonium states at a fixed temperature, $T = 0.175$ GeV. For the J/ψ resonance, ρ_{00} increases with C , whereas a slight decreasing trend is observed for $\psi(2S)$. In the case of $\Upsilon(1S)$ and $\Upsilon(2S)$, ρ_{00} increases monotonically with increasing C . These observations demonstrate that the spin alignment behavior varies across different quarkonium states, despite all being vector mesons. This variation primarily arises due to differences in meson mass and the consequent changes in eigenenergy under the influence of vorticity. As discussed in Fig. 2, among all the resonances, Fig. 4 depicts a clear sensitivity of $\Upsilon(1S)$, and $\Upsilon(2S)$ state to the circulation parameter C . For $C < 0.8$ fm, J/ψ exhibits a higher degree of spin alignment than the other mesons. Conversely, $\Upsilon(2S)$ displays the lowest spin alignment at $C = 0.8$ fm, with $\rho_{00} \sim \frac{1}{3}$, which can be ascribed to its relatively large mass and comparable eigen energies for three spin projection states. Moreover, the findings suggest that increasing vorticity has a pronounced effect on the energy eigenstates of heavier particles and therefore reinforces their spin alignment. Consequently, for $C > 0.8$ fm, the spin alignment of $\Upsilon(1S)$ and $\Upsilon(2S)$ surpasses charmonium counterpart J/ψ and $\psi(2S)$, respectively.

Besides the vorticity, a strong magnetic field is considered to be produced in the heavy-ion collisions and is expected to affect the spin alignment of vector mesons [77]. Since heavy quarks (charm and/or beauty) are primarily produced at the early stage of heavy-ion collisions, the initially generated magnetic field is anticipated to polarize the heavy quarks. Hence, heavy quarks can be considered a crucial probe to

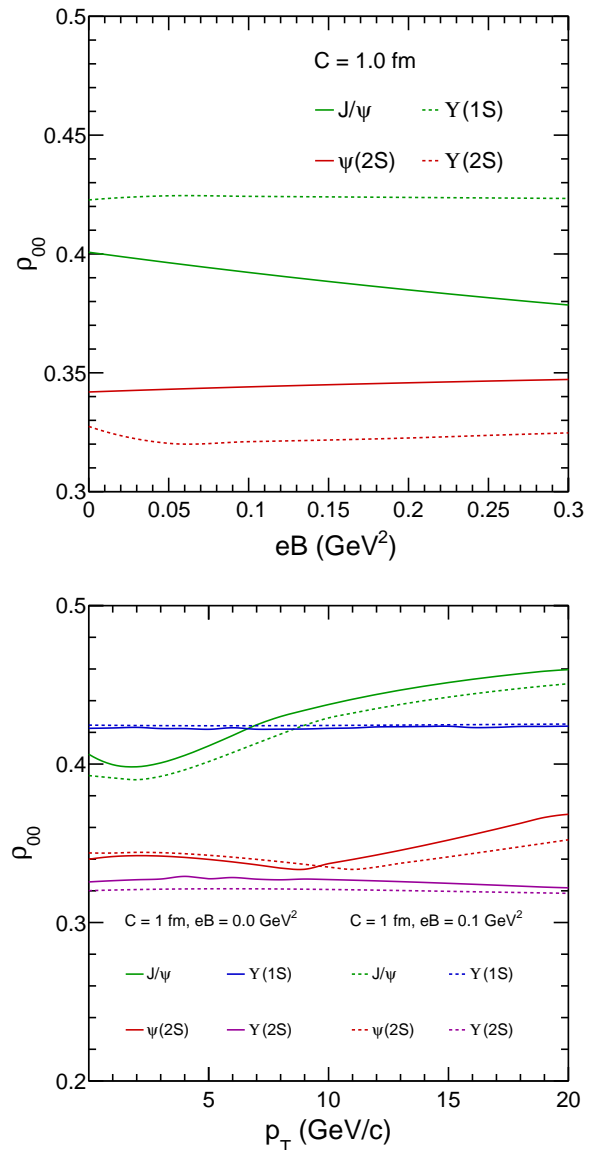


FIG. 5. (Color online) The spin alignment observable ρ_{00} as a function of p_T (upper panel) and magnetic field eB (lower panel) for J/ψ , $\psi(2S)$, $\Upsilon(1S)$, and $\Upsilon(2S)$ states at $C = 1.0$ fm using $T = 0.175$ GeV.

study the spin dynamics and magnetic field effect in ultra-relativistic heavy-ion collisions. In Fig. 5, we investigate the initial state dynamics, such as the effect of rotation and magnetic field on the spin alignment observables. The interplay of coupling of spin with rotation ($\boldsymbol{\omega} \cdot \mathbf{S}$) and magnetic field ($\boldsymbol{\mu} \cdot \mathbf{B}$, where $\boldsymbol{\mu} = g \frac{q}{2m} \mathbf{S}$), is examined through the spin density matrix element ρ_{00} .

The upper panel of Fig. 5 shows ρ_{00} as a function of eB at $C = 1.0$ fm and $T = 0.175$ GeV for 1S and 2S quarkonium states. Our study predicts a nominal decrease in the order of spin alignment for J/ψ with an increasing magnetic field. While the spin alignment of

$\psi(2S)$ almost remains invariant with the magnetic field. The magnetic field is found to marginally affect the spin alignment of $\Upsilon(1S)$ as the magnitude of ρ_{00} remains almost constant with the magnetic field. Likewise, the $\Upsilon(2S)$ also seems to be largely unaffected by the magnetic field and left unpolarized as ρ_{00} for $\Upsilon(2S)$ closely varies around $1/3$. The change in ρ_{00} for all the chosen quarkonium states with eB follows a similar explanation as Fig. 4, where the eigenenergy was enhanced due to temperature, and here the magnetic field does the same. Unlike Fig. 4, the subtle behavior ρ_{00} can be considered as an artifact of the change brought to the coupling constant, $\alpha_s(\Lambda^2, eB)$, in the presence of the magnetic field.

The lower panel of Fig. 5 illustrates ρ_{00} as a function of p_T at $C = 1.0$ fm. It is shown to quantify the impact of the magnetic field on the spin alignment of various quarkonium states. Therefore, it is shown for two cases; the solid line depicts the presence of a magnetic field $eB = 0.1$ GeV², whereas the dashed line shows ρ_{00} in the absence of the magnetic field. As the degree of spin-alignment quantified in terms of the deviation of ρ_{00} from $1/3$ is decreased for J/ψ due to the magnetic field in the whole p_T ranges, while for $\psi(2S)$, the deviation of ρ_{00} from $1/3$ due to the magnetic field seems to slightly increase at lower p_T . Interestingly, the magnetic field increases the absolute degree of spin-alignment (i.e., $|\rho_{00} - 1/3|$) for $\Upsilon(1S)$ and $\Upsilon(2S)$ states oppositely. For $\Upsilon(1S)$ state ρ_{00} is greater than $1/3$, while for $\Upsilon(2S)$ state ρ_{00} is less than $1/3$. It suggests that, depending on the binding energy of the quarkonium state, the effect of the magnetic field on the spin alignment of the respective state varies accordingly. Here, it is noteworthy to mention the time scale at which quarkonia couple (align) to the vortex (rotation), and the magnetic field of the medium may not necessarily be at the same time. The estimation of the relaxation time for quarkonium spin alignment with the local flow gradients is required for a comprehensive study.

As discussed in Section II B, anisotropy in the medium is expected to influence the spin alignment of vector mesons [77]. This effect is explored in Fig. 6, which shows how the spin density matrix element ρ_{00} varies with the anisotropy parameter ξ . The upper panel of Fig. 6 presents ρ_{00} as a function of ξ for quarkonium, considering it at rest in the medium, with $C = 1.0$ fm and $T = 0.175$ GeV. For small anisotropies ($\xi < 0.2$), a decrease in spin alignment is observed for the J/ψ , while the $\psi(2S)$ shows only a marginal effect, with a slight enhancement. At higher anisotropy values ($\xi > 0.2$), ρ_{00} for J/ψ increases, whereas for $\psi(2S)$, it initially decreases before reaching a saturation point. In contrast, the heavier bottomonium states, $\Upsilon(1S)$ and $\Upsilon(2S)$, show negligible variation in ρ_{00} across the entire range of ξ , indicating that their spin alignment is largely unaffected by the momentum-space anisotropy.

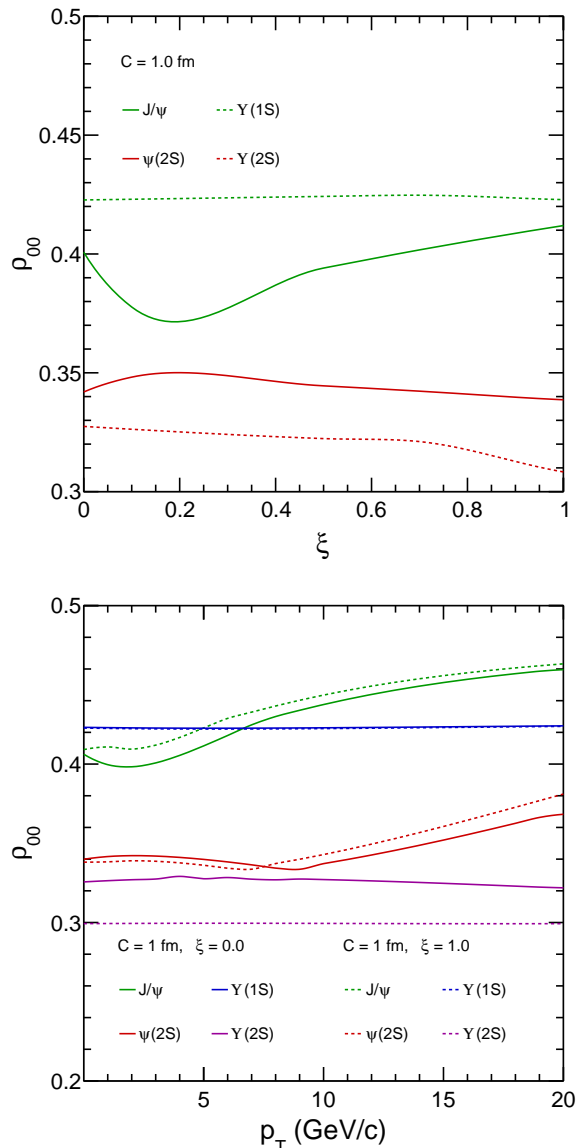


FIG. 6. (Color online) The spin alignment observable ρ_{00} as a function of p_T (upper panel) and medium anisotropy ξ (lower panel) for J/ψ , $\psi(2S)$, $\Upsilon(1S)$, and $\Upsilon(2S)$ states at $C = 1.0$ fm using $T = 0.175$ GeV.

The lower panel of Fig. 6 presents ρ_{00} as a function of p_T for various quarkonium states, again at $C = 1.0$ fm. Two scenarios are compared: solid lines represent an anisotropic medium with $\xi = 1.0$, and dashed lines denote the isotropic case ($\xi = 0$). The results reinforce that the impact of anisotropy is state-dependent. For the J/ψ , the deviation of ρ_{00} from the isotropic baseline of $1/3$ increases across all p_T values in the anisotropic case. Conversely, the $\psi(2S)$ shows a slight decrease in deviation at low p_T . The $\Upsilon(1S)$ state remains largely unaffected by either anisotropy or transverse momentum, while for $\Upsilon(2S)$, a small but consistent shift in ρ_{00} is

observed in the presence of anisotropy. These findings stress the significance of medium-induced momentum-space anisotropy in modifying the spin alignment of lighter vector mesons. While the effects are modest, they are measurable and offer insights into the early-stage dynamics of the quark-gluon plasma. However, the influence of anisotropy appears minimal for heavier states such as bottomonium, suggesting that their spin alignment serves as a more robust probe that is less sensitive to such medium effects.

B. Off-diagonal elements

Furthermore, it is proposed that apart from the diagonal elements of the spin density matrix ρ_{00} , the off-diagonal elements of the spin density matrix provide crucial information about the dynamics of the system produced in heavy-ion collisions. Such as the off-diagonal elements help to differentiate the local spin alignment of vector mesons from the global one. Studying these observables provides key insights about the spin hydrodynamic evolution in heavy-ion collision and the freeze-out dynamics, etc [63, 66–68]. It is proposed that the off-diagonal spin density matrix elements provide valuable insights into medium-induced spin correlations, quantum coherence, the local spin structure, and non-equilibrium QCD dynamics [100]. Similar to diagonal elements, one can obtain the off-diagonal matrix elements of the spin–density matrix in a rotating frame, such as $\rho_{1,-1}$, $\rho_{-1,0}$, and $\rho_{1,0}$ and is expressed as follows;

1. $\rho_{1,-1}^r$

$$\rho_{1,-1}^r = \frac{\sin^2 \theta_r}{4Z} (\rho_{1,1} + e^{-2i\phi_r} \rho_{-1,-1} + 2e^{-i\phi_r} \rho_{0,0}) \quad (33)$$

At $\phi_r = 0$, we have

$$\text{Re}[\rho_{1,-1}^r] = \frac{\sin^2 \theta_r}{4Z} (\rho_{1,1} + \rho_{-1,-1} + 2\rho_{0,0}) \quad (34)$$

Using the relation, $\rho_{1,1} + \rho_{0,0} + \rho_{-1,-1} = 1$, we have

$$\text{Re}[\rho_{1,-1}^r] = \frac{\sin^2 \theta_r}{4Z} (1 + \rho_{0,0}) \quad (35)$$

2. $\rho_{-1,0}^r$

$$\rho_{-1,0}^r = \frac{\sin \theta_r}{Z 2\sqrt{2}} \left[(1 - \cos \theta_r) e^{2i\phi_r} \rho_{1,1} + 2 \cos \theta_r e^{i\phi_r} \rho_{0,0} + (1 + \cos \theta_r) \rho_{-1,-1} \right] \quad (36)$$

At $\phi_r = 0$, we have

$$\text{Re}[\rho_{-1,0}^r] = \frac{\sin \theta_r}{Z 2\sqrt{2}} \left[(1 - \cos \theta_r) \rho_{1,1} + 2 \cos \theta_r \rho_{0,0} - (1 + \cos \theta_r) \rho_{-1,-1} \right] \quad (37)$$

3. $\rho_{1,0}^r$

$$\rho_{1,0}^r = \frac{\sin \theta_r}{Z 2\sqrt{2}} \left[(1 + \cos \theta_r) \rho_{1,1} - 2 \cos \theta_r e^{i\phi_r} \rho_{0,0} - (1 - \cos \theta_r) e^{-2i\phi_r} \rho_{-1,-1} \right] \quad (38)$$

At $\phi_r = 0$, we have

$$\text{Re}[\rho_{1,0}^r] = \frac{\sin \theta_r}{Z 2\sqrt{2}} \left[(1 + \cos \theta_r) \rho_{1,1} - 2 \cos \theta_r \rho_{0,0} - (1 - \cos \theta_r) \rho_{-1,-1} \right] \quad (39)$$

Consequently, we explore the off-diagonal elements of the spin-density matrix, i.e., $\rho_{1,-1}$, $\rho_{-1,0}$, and $\rho_{1,0}$ in this section. The studied off-diagonal matrix elements appear as coefficients of the angular distribution of the decay daughter in the mother particle's rest frame. These coefficients are used as a proxy to measure the local polarization of the relativistic fluid. Figure. 7 shows real part of the $\rho_{1,-1}$, $\rho_{-1,0}$, and $\rho_{1,0}$ matrix elements as a function of p_T for J/ψ , $\psi(2S)$, $\Upsilon(1S)$, and $\Upsilon(2S)$ states. The non-zero values of the off-diagonal elements in Fig. 7 indicate that the system is in a mixed ensemble state and characterized by the quantum superposition between the quantum elements. As a result, the quantum coherence (decoherence) can be inferred from the spin-density matrix. On average, we found $\text{Re}[\rho_{1,-1}]$, $\text{Re}[\rho_{-1,0}]$, and $\text{Re}[\rho_{1,0}]$ have qualitatively similar trends as a function of p_T , except a change in the magnitude is observed as a function of p_T . It is observed that $\text{Re}[\rho_{1,-1}]$ is always positive, while $\text{Re}[\rho_{-1,0}]$ and $\text{Re}[\rho_{1,0}]$ is always negative for all quarkonium states. Similar to ρ_{00} , $\Upsilon(1S)$ and $\Upsilon(2S)$ states have a very marginal effect on these off-diagonal matrix elements as a function of p_T . However, for J/ψ and $\psi(2S)$, $\text{Re}[\rho_{1,-1}]$, $\text{Re}[\rho_{-1,0}]$, and $\text{Re}[\rho_{1,0}]$ show a decreasing trend at high p_T . The correlation between the different spin projections is reflected in these off-diagonal matrix elements. It is proposed that both the local and long-range correlations can be estimated by studying the spin density matrix. Figure. 8 and Fig. 9 depict the real part of $\rho_{1,-1}$, $\rho_{-1,0}$, and $\rho_{1,0}$ matrix elements as a function of temperature T and circulation parameter C , respectively, for J/ψ , $\psi(2S)$, $\Upsilon(1S)$, and $\Upsilon(2S)$ states. Moreover, as presented in the study, the temperature and vorticity dependence of these off-diagonal elements reveal how the thermal and rotational characteristics of the medium impact the spin coherence. For example, we found $\rho_{-1,0}$ and

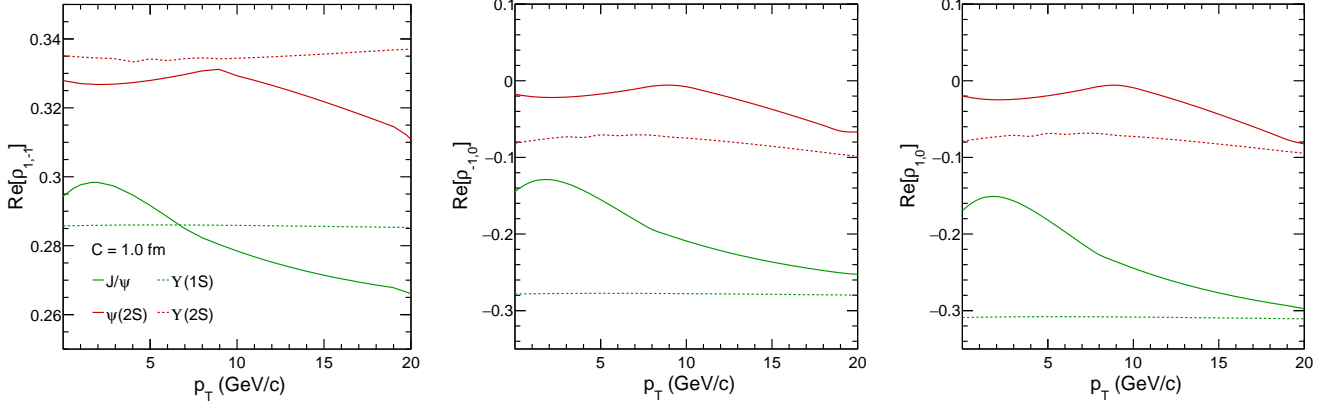


FIG. 7. (Color online) The off-diagonal elements of the spin density matrix, such as $\text{Re}[\rho_{1,-1}]$ (left panel), $\text{Re}[\rho_{-1,0}]$ (middle panel), and $\text{Re}[\rho_{1,0}]$ (right panel) as a functions of p_T for J/ψ , $\psi(2S)$, $\Upsilon(1S)$, and $\Upsilon(2S)$ states at $C = 1$ fm and $T = 0.175$ GeV.

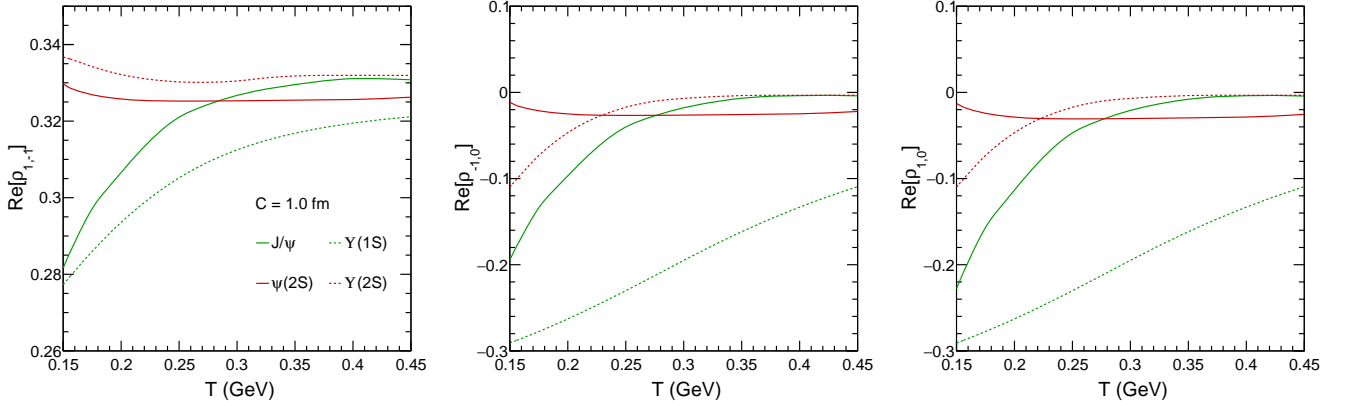


FIG. 8. (Color online) The off-diagonal elements of the spin density matrix, such as $\text{Re}[\rho_{1,-1}]$ (left panel), $\text{Re}[\rho_{-1,0}]$ (middle panel), and $\text{Re}[\rho_{1,0}]$ (right panel) as a function of temperature T for J/ψ , $\psi(2S)$, $\Upsilon(1S)$, and $\Upsilon(2S)$ states at $C = 1$ fm.

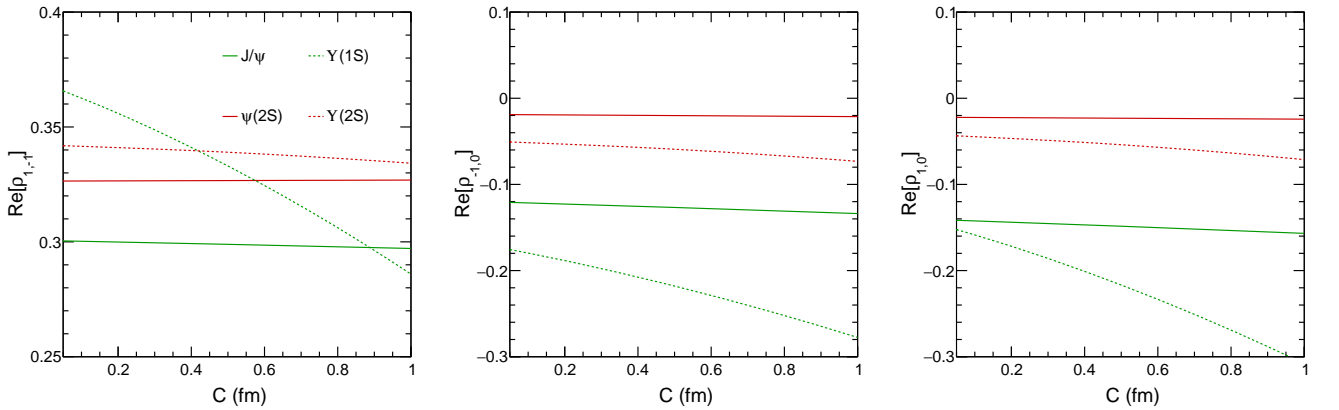


FIG. 9. (Color online) The off-diagonal elements of the spin density matrix, such as $\text{Re}[\rho_{1,-1}]$ (left panel), $\text{Re}[\rho_{-1,0}]$ (middle panel), and $\text{Re}[\rho_{1,0}]$ (right panel) as a function of circulation parameter C for J/ψ , $\psi(2S)$, $\Upsilon(1S)$, and $\Upsilon(2S)$ states at $T = 0.175$ GeV.

$\rho_{1,0}$ approach towards zero with increasing temperature, reflecting a loss of quantum coherence at high tempera-

ture. Conversely, with increasing the circulation parameter C , which quantifies the vorticity of the medium, the

magnitude of the off-diagonal elements for $\Upsilon(1S)$ is enhanced (baseline is zero), whereas charmonium states as well as $\Upsilon(2S)$ are marginally affected. This trend confirms that rotational effects promote quantum coherence between spin states, and hence, spin alignment is more pronounced in a thermo-vortical medium.

IV. SUMMARY

In this work, we have studied the spin alignment of J/ψ , $\psi(2S)$, $\Upsilon(1S)$, and $\Upsilon(2S)$ states in a deconfined thermalized magneto-vortical medium in the presence of momentum-space anisotropy. The important findings of this paper are summarized below:

1. We explore the effect of vorticity, quantified in terms of the circulation parameter C , on the spin alignment of J/ψ , $\psi(2S)$, $\Upsilon(1S)$, and $\Upsilon(2S)$ states by obtaining the vorticity and different spin projections dependent energy eigenvalues. We use a medium-modified color-singlet potential model of quarkonia to estimate the medium temperature, vorticity, magnetic field, and medium momentum space anisotropy dependent on the energy eigenvalues by solving the Schrödinger equation. Furthermore, the energy eigenvalues are used to calculate the diagonal element ρ_{00} , and the off-diagonal elements such as $\rho_{1,-1}$, $\rho_{-1,0}$, and $\rho_{1,0}$ of the spin-density matrix for J/ψ , $\psi(2S)$, $\Upsilon(1S)$, and $\Upsilon(2S)$ states in a rotating frame.
2. The deviation of $\rho_{00}^{J/\psi}$ from 1/3 indicate that the distribution of the produced J/ψ in relativistic heavy-ion collisions is not isotropic. In our study, $\rho_{00}^{J/\psi}$ is found to be always greater than 1/3 for all considered values of C and p_T ranges. However, the recent experimental measurement shows ρ_{00} is observed to be less than 1/3 at low p_T and greater than 1/3 at high p_T in Pb+Pb collisions at $\sqrt{s_{NN}} = 5.02$ TeV [27, 36, 37]. The experimentally measured polarization parameters λ_θ are connected to the diagonal element ρ_{00} of the spin-density via the relation; $\rho_{00} = \frac{1-\lambda_\theta}{3+\lambda_\theta}$. If $\lambda_\theta < 0$, then $\rho_{00} > 1/3$ and vice-versa. The other polarization parameters λ_ϕ and $\lambda_{\theta\phi}$ are related to the off-diagonal elements of the spin density matrix, and the explicit relation can be found in Ref. [66]. Interestingly, similar to our findings of ρ_{00} for J/ψ , and $\psi(2S)$ the increasing behavior of ρ_{00} with p_T and large polarization is also observed for other heavy flavor hadrons such as D^{*+} in Pb+Pb collisions at $\sqrt{s_{NN}} = 5.02$ TeV[8, 27]. This hints at a common physics mechanism responsible for the spin alignment of heavy-flavor hadrons, and these heavy-flavor hadrons act as better probes for spin alignment studies in relativistic heavy-ion collisions.
3. We found the ρ_{00} observable for bottomonium states, specifically $\Upsilon(1S)$ state, has pronounced effect ($\rho_{00} < 1/3$ at low C and $\rho_{00} > 1/3$ at high C) of medium vorticity compared to the charmonium states. A similar feature is also seen for the $\Upsilon(2S)$ state as a function of C . This implies that the shape of the angular distribution depends strongly on the initial anisotropy that arises due to rotation. The value of vorticity, at which the shape of the angular distribution changes, is highly sensitive to the temperature and equilibration time of the quark-gluon plasma. Hence, the spin alignment of the bottomonium state may serve as a probe of system thermalization.
4. The effect of temperature, magnetic field, and medium momentum-space anisotropy on ρ_{00} observable is explored because the energy eigenvalues change with these parameters. The magnetic field and medium anisotropies affect the quarkonium states in a state-dependent manner. The possible reason for the state-dependent behavior of ρ_{00} in the presence of a magnetic field and medium anisotropy could be due to their different size, mass, binding energy, etc. Therefore, it is observed that the binding energy (mass) and melting temperature (width) of quarkonium states are sensitive to the medium temperature, rotation, magnetic field, and anisotropy parameters. In addition, it is expected that the coupling strength and the time scale at which the bottom and charm quarks will align with the magnetic field and the anisotropy direction will be different. This may affect the spin alignment observables of different quarkonium states.
5. The non-vanishing value of the off-diagonal elements of the spin-density matrix, such as $\rho_{1,-1}$, $\rho_{-1,0}$, and $\rho_{1,0}$, reflects the possible coherence between different spin states. This could be due to the final state interaction of the vector mesons. From a theoretical standpoint, the non-zero off-diagonal elements are essential for modeling spin-hydrodynamic evolution and refining hadronization mechanisms that incorporate spin effects. These off-diagonal elements provide constraints for quantum kinetic theories, particularly those involving Wigner functions and spin-vorticity coupling, and offer a route to quantify spin relaxation time scales in QGP. These elements also serve as probes of non-equilibrium QCD dynamics, especially in regions where momentum-space anisotropy or magnetic fields perturb local thermodynamic equilibrium. Altogether, while ρ_{00} determines the magnitude of spin alignment along a quantization axis, the off-diagonal components describe the full three-dimensional structure of the spin distribution, including angular correlations and coherence effects. Their behavior encodes subtle features of the QGP medium, such as its degree of thermalization, rota-

tional structure, and local spin dynamics. Understanding and measuring these elements experimentally can thus unlock deeper insights into the collective behavior of the QGP and the fundamental mechanisms of spin transport in strongly interacting matter.

6. It is important to note that apart from the studied sources, there could be various potential sources and physics mechanisms responsible for the spin-alignment of quarkonium states. Such as the correlations and fluctuations of strong force field between the quark and anti-quark pairs [69], turbulent color field [71, 72], electric field [61, 65], fragmentation process [60], local spin alignment and helicity [63, 64], etc. The contribution of each source to the spin alignment of quarkonium states requires more examination.

Apart from the degree of alignment of different hadrons, the spin alignment measurement in heavy-ion collisions provides various other crucial features of the system. Such as the ρ_{00} elements affect the experimentally measurable chiral magnetic effect (CME) sensitive observables, including γ_{112} correlator, $R_{\Psi_2}(\Delta S)$ corre-

lator, and signed balance function, etc. [101]. Furthermore, ρ_{00} observable helps to find the correlations and fluctuations of the strong force field in the quarkonium states as it is linked to the fundamental properties of QCD. Quarkonium polarization could be a promising observable to probe the spin hydrodynamics and freeze-out properties in the quark-gluon plasma. So far, the spin alignment of various vector mesons across collision systems and energies remains challenging and not described by a common physics mechanism. Thus, an intense investigation of the spin alignment of vector mesons is required from both experimental and theoretical perspectives. With the current high statistics, the Run 3 data samples of LHC experiments, a more differential and precise measurement can be performed on the local and global spin alignment of various vector mesons (including strange, charm, and bottom sectors).

ACKNOWLEDGEMENT

Bhagyarathi Sahoo acknowledges the financial aid from CSIR, Government of India. The authors gratefully acknowledge the DAE-DST, Government of India, funding under the mega-science project "Indian Participation in the ALICE experiment at CERN" bearing Project No. SR/MF/PS-02/2021-IITI (E-37123).

-
- [1] J. Adam *et al.* [ALICE Collaboration], *Nature Phys.* **13**, 535 (2017).
 - [2] V. Khachatryan *et al.* [CMS Collaboration], *Phys. Lett. B* **765**, 193 (2017).
 - [3] A. Ortiz Velasquez, P. Christiansen, E. Cuautle Flores, I. Maldonado Cervantes and G. Paic, *Phys. Rev. Lett.* **111**, 042001 (2013).
 - [4] C. Zhang, A. Behera, S. Bhatta and J. Jia, *Phys. Lett. B* **822**, 136702 (2021).
 - [5] S. Prasad, B. Sahoo, S. Tripathy, N. Mallick and R. Sahoo, *Phys. Rev. C* **111**, 044902 (2025).
 - [6] M. Coquet, M. Winn, X. Du, J. Y. Ollitrault and S. Schlichting, *Phys. Rev. Lett.* **132**, 232301 (2024).
 - [7] X. Y. Wu, H. Gao, B. Forster, C. Gale, G. Jackson and S. Jeon, [arXiv:2412.15052].
 - [8] S. Dey and A. Jaiswal, [arXiv:2502.20352].
 - [9] B. Sahoo, D. Sahu, S. Deb, C. R. Singh and R. Sahoo, *Phys. Rev. C* **109**, 034910 (2024).
 - [10] L. Adamczyk *et al.* [STAR Collaboration], *Nature* **548**, 62 (2017).
 - [11] J. Adam *et al.* [STAR Collaboration], *Phys. Rev. C* **98**, 014910 (2018).
 - [12] S. Acharya *et al.* [ALICE Collaboration], *Phys. Rev. C* **101** (2020) no.4, 044611 [erratum: *Phys. Rev. C* **105** (2022) no.2, 029902].
 - [13] J. Adam *et al.* [STAR Collaboration], *Phys. Rev. Lett.* **126**, 162301 (2021).
 - [14] J. Adam *et al.* [STAR Collaboration], *Phys. Rev. Lett.* **123**, 132301 (2019).
 - [15] S. Acharya *et al.* [ALICE Collaboration], *Phys. Rev. Lett.* **128**, 172005 (2022).
 - [16] M. Abdulhamid *et al.* [STAR Collaboration], *Phys. Rev. Lett.* **131**, 202301 (2023).
 - [17] Y. Xie, D. Wang and L. P. Csernai, *Phys. Rev. C* **95**, 031901 (2017).
 - [18] S. Ryu, V. Jupic and C. Shen, *Phys. Rev. C* **104**, 054908 (2021).
 - [19] B. Fu, K. Xu, X. G. Huang and H. Song, *Phys. Rev. C* **103**, 024903 (2021).
 - [20] D. X. Wei, W. T. Deng and X. G. Huang, *Phys. Rev. C* **99**, 014905 (2019).
 - [21] F. Becattini, M. Buzzegoli, G. Inghirami, I. Karpenko and A. Palermo, *Phys. Rev. Lett.* **127**, 272302 (2021).
 - [22] B. Sahoo, C. R. Singh and R. Sahoo, [arXiv:2404.15138].
 - [23] B. I. Abelev *et al.* [STAR Collaboration], *Phys. Rev. C* **77**, 061902 (2008).
 - [24] M. S. Abdallah *et al.* [STAR Collaboration], *Nature* **614**, 244 (2023).
 - [25] S. Acharya *et al.* [ALICE Collaboration], *Phys. Rev. Lett.* **125**, 012301 (2020).
 - [26] S. Acharya *et al.* [ALICE Collaboration], *Phys. Lett. B* **846**, 137920 (2023).
 - [27] S. Acharya *et al.* [ALICE Collaboration], [arXiv:2504.00714].
 - [28] L. Adamczyk *et al.* [STAR Collaboration], *Phys. Lett. B* **739**, 180 (2014).
 - [29] J. Adam *et al.* [STAR Collaboration], *Phys. Rev. D* **102**, 092009 (2020).

- [30] S. Chatrchyan *et al.* [CMS Collaboration], Phys. Lett. B **727**, 381 (2013).
- [31] B. Abelev *et al.*, [ALICE Collaboration], Phys. Rev. Lett. **108**, 082001 (2012).
- [32] S. Acharya *et al.*, [ALICE Collaboration], Eur. Phys. J. C **78**, 562 (2018).
- [33] S. Chatrchyan *et al.* [CMS Collaboration], Phys. Rev. Lett. **110**, 081802 (2013).
- [34] R. Aaij *et al.*, [LHCb Collaboration], Eur. Phys. J. C **73**, 2631 (2013).
- [35] R. Aaij *et al.* [LHCb Collaboration], Eur. Phys. J. C **74**, 2872 (2014).
- [36] S. Acharya *et al.* [ALICE Collaboration], Phys. Lett. B **815**, 136146 (2021).
- [37] S. Acharya *et al.* [ALICE Collaboration], Phys. Rev. Lett. **131**, 042303 (2023).
- [38] B. Betz, M. Gyulassy and G. Torrieri, Phys. Rev. C **76**, 044901 (2007).
- [39] X. L. Xia, H. Li, Z. B. Tang and Q. Wang, Phys. Rev. C **98**, 024905 (2018).
- [40] B. Sahoo, C. R. Singh, D. Sahu, R. Sahoo and J. e. Alam, Eur. Phys. J. C **83**, 873 (2023).
- [41] A. Einstein and W. J. de Haas, Verh. Dtsch. Phys. Ges. **17**, 152 (1915).
- [42] F. Becattini, I. Karpenko, M. Lisa, I. Uppsal and S. Voloshin, Phys. Rev. C **95**, 054902 (2017).
- [43] Z. F. Jiang, X. Y. Wu, S. Cao and B. W. Zhang, Phys. Rev. C **108**, 064904 (2023).
- [44] V. Skokov, A. Y. Illarionov and V. Toneev, Int. J. Mod. Phys. A **24**, 5925 (2009).
- [45] K. K. Pradhan, B. Sahoo, D. Sahu and R. Sahoo, Eur. Phys. J. C **84**, 936 (2024).
- [46] B. Sahoo, K. K. Pradhan, D. Sahu and R. Sahoo, Phys. Rev. D **108**, 074028 (2023).
- [47] C. W. Aung, A. Dwibedi, J. Dey and S. Ghosh, Phys. Rev. C **109**, 2024 (2024).
- [48] A. Dwibedi, C. W. Aung, J. Dey and S. Ghosh, Phys. Rev. C **109**, 034914 (2024).
- [49] S. Wu and Y. Xie, Eur. Phys. J. A **59**, 108 (2023).
- [50] Z. Z. Han and J. Xu, Phys. Lett. B **786**, 255 (2018).
- [51] K. Xu, F. Lin, A. Huang and M. Huang, Phys. Rev. D **106**, L071502 (2022).
- [52] L. Dong, Y. Guo, A. Islam and M. Strickland, Phys. Rev. D **104**, 096017 (2021).
- [53] P. Romatschke, Phys. Rev. C **75**, 014901 (2007); P. Romatschke and M. Strickland, Phys. Rev. D **71**, 125008 (2005).
- [54] B. Schenke and M. Strickland, Phys. Rev. D **76**, 025023 (2007).
- [55] M. Martinez and M. Strickland, Phys. Rev. Lett. **100**, 102301 (2008); Phys. Rev. C **78**, 034917 (2008).
- [56] A. Dumitru, Y. Nara, B. Schenke and M. Strickland, Phys. Rev. C **78**, 024909 (2008).
- [57] R. Baier and Y. Mehtar-Tani, Phys. Rev. C **78**, 064906 (2008).
- [58] A. Dumitru, Y. Guo and M. Strickland, Phys. Lett. B **662**, 37 (2008).
- [59] M. E. Carrington, A. Rebhan, Phys. Rev. D **79**, 025018 (2009).
- [60] Z. T. Liang and X. N. Wang, Phys. Lett. B **629**, 20 (2005).
- [61] Y. G. Yang, R. H. Fang, Q. Wang and X. N. Wang, Phys. Rev. C **97**, 034917 (2018).
- [62] X. L. Sheng, Q. Wang and X. N. Wang, Phys. Rev. D **102**, 056013 (2020).
- [63] X. L. Xia, H. Li, X. G. Huang and H. Zhong Huang, Phys. Lett. B **817**, 136325 (2021).
- [64] J. H. Gao, Phys. Rev. D **104**, 076016 (2021).
- [65] X. L. Sheng, L. Oliva and Q. Wang, Phys. Rev. D **101**, 096005 (2020). [erratum: Phys. Rev. D **105**, 099903 (2022).]
- [66] K. J. Goncalves and G. Torrieri, Phys. Rev. C **105**, 034913 (2022).
- [67] P. H. De Moura, K. J. Goncalves and G. Torrieri, Phys. Rev. D **108**, 034032 (2023).
- [68] K. J. Goncalves, G. Torrieri and R. Ryblewski, [arXiv:2410.16448].
- [69] X. L. Sheng, L. Oliva, Z. T. Liang, Q. Wang and X. N. Wang, Phys. Rev. Lett. **131**, 042304 (2023).
- [70] J. p. Lv, Z. h. Yu, Z. t. Liang, Q. Wang and X. N. Wang, Phys. Rev. D **109**, 114003 (2024).
- [71] A. Kumar, B. Müller and D. L. Yang, Phys. Rev. D **108**, 016020 (2023).
- [72] B. Müller and D. L. Yang, Phys. Rev. D **105**, L011901 (2022). [erratum: Phys. Rev. D **106**, 039904 (2022).]
- [73] B. Fu, F. Gao, Y. X. Liu and H. Song, Phys. Lett. B **855**, 138821 (2024).
- [74] K. Xu and M. Huang, Phys. Rev. D **110**, 094034 (2024).
- [75] Y. Q. Zhao, X. L. Sheng, S. W. Li and D. Hou, JHEP **08**, 070 (2024).
- [76] X. L. Sheng, Y. Q. Zhao, S. W. Li, F. Becattini and D. Hou, Phys. Rev. D **110**, 056047 (2024).
- [77] B. Sahoo, C. R. Singh and R. Sahoo, Eur. Phys. J. C **85**, 580 (2025).
- [78] J. H. Chen, Z. T. Liang, Y. G. Ma, X. L. Sheng and Q. Wang, Sci. China Phys. Mech. Astron. **68** 211001 (2025).
- [79] C. R. Singh, S. Ganesh and M. Mishra, Eur. Phys. J. C **79**, 147 (2019).
- [80] C. R. Singh, S. Deb, R. Sahoo and J. e. Alam, Eur. Phys. J. C **82**, 542 (2022).
- [81] C. R. Singh, P. Bagchi, R. Sahoo and J. e. Alam, [arXiv:2501.00753] (Phys. Rev. D: In Press).
- [82] C. R. Singh, P. K. Srivastava, S. Ganesh and M. Mishra, Phys. Rev. C **92**, 034916 (2015).
- [83] S. Ganesh, C. R. Singh and M. Mishra, J. Phys. G **45**, 035003 (2018).
- [84] N. Hatwar, C. R. Singh, S. Ganesh and M. Mishra, Phys. Rev. C **104**, 034905 (2021).
- [85] Anandan, J., Suzuki, J. (n.d.). Quantum Mechanics in a Rotating Frame. <https://doi.org/https://arxiv.org/pdf/quant-ph/0305081.pdf>
- [86] Gordan Baym, Lectures on Quantum Mechanics (1969). <https://archive.org/details/lecturesonquantu0000baym/page/n611/mode/2up>
- [87] David J. Griffiths, Introduction to Quantum Mechanics. <https://www.fisica.net/mecanica-quantica/Griffiths%20-%20Introduction%20to%20quantum%20mechanics.pdf>
- [88] F. Nendzig and G. Wolschin, Phys. Rev. C **87**, 024911 (2013).
- [89] J. Hoelck, F. Nendzig and G. Wolschin, Phys. Rev. C **95**, 024905 (2017).
- [90] F. Nendzig and G. Wolschin, J. Phys. G **41**, 095003 (2014).
- [91] H. X. Zhang, J. W. Kang and B. W. Zhang, Eur. Phys. J. C **81**, 623 (2021).

- [92] B. Karmakar, A. Bandyopadhyay, N. Haque and M. G. Mustafa, *Eur. Phys. J. C* **79**, 658 (2019).
- [93] A. Ayala, C. A. Dominguez, S. Hernandez-Ortiz, L. A. Hernandez, M. Loewe, D. Manreza Paret and R. Zamora, *Phys. Rev. D* **98**, 031501 (2018).
- [94] A. Bandyopadhyay, B. Karmakar, N. Haque and M. G. Mustafa, *Phys. Rev. D* **100**, 034031 (2019).
- [95] L. Dong, Y. Guo, A. Islam, A. Rothkopf and M. Strickland, *JHEP* **09**, 200 (2022).
- [96] M. Strickland and D. Bazow, *Nucl. Phys. A* **879**, 25-58 (2012).
- [97] P. Romatschke and M. Strickland, *Phys. Rev. D* **68**, 036004 (2003).
- [98] P. Romatschke and M. Strickland, *Phys. Rev. D* **70**, 116006 (2004).
- [99] M. Strickland, *Anisotropic hydrodynamics: Three lectures*, *Acta Phys. Pol. B* 45, 2355 (2014).
- [100] M. Anselmino, P. Kroll and B. Pire, *Z. Phys. C* **29**, 135 (1985).
- [101] D. Shen, J. Chen, A. Tang and G. Wang, *Phys. Lett. B* **839**, 137777 (2023).